

Reconfigurable Intelligent Surface Empowered Device-to-Device Communication Underlying Cellular Networks

Gang Yang, *Member, IEEE*, Yating Liao, *Student Member, IEEE*, Ying-Chang Liang, *Fellow, IEEE*, and Olav Tirkkonen, *Member, IEEE*

Abstract

Reconfigurable intelligent surface (RIS) is a new and revolutionary technology to achieve spectrum-, energy- and cost-efficient wireless networks. This paper studies the resource allocation for RIS-empowered device-to-device (D2D) communication underlying a cellular network, in which an RIS is employed to enhance desired signals and suppress interference between paired D2D and cellular links. We maximize the overall network's spectrum efficiency (SE) (i.e., sum rate of D2D users and cellular users) and energy efficiency (EE), respectively, by jointly optimizing the resource reuse indicators, the transmit power and the RIS's passive beamforming, under the signal-to-interference-plus-noise ratio constraints and other practical constraints. To solve the non-convex problems, we first propose an efficient user-pairing scheme based on relative channel strength to determine the resource reuse indicators. Then, the transmit power and the RIS's passive beamforming are jointly optimized to maximize the SE by a proposed iterative algorithm, based on the techniques of alternating optimization, successive convex approximation, Lagrangian dual transform and quadratic transform. Moreover, the EE-maximization problem is solved by an alternating algorithm integrated with Dinkelbach's method. Also, the convergence and complexity of both algorithms are analyzed. Numerical results show that the proposed design achieves significant SE and EE enhancements compared to traditional underlying D2D network without RIS and other benchmarks.

Index Terms

Device-to-device communication, reconfigurable intelligent surface, spectrum efficiency optimization, energy efficiency optimization, resource allocation, passive beamforming.

G. Yang and Y. Liao are with the National Key Laboratory of Science and Technology on Communications, and the Center for Intelligent Networking and Communications (CINC), University of Electronic Science and Technology of China (UESTC), Chengdu 611731, China (e-mails: yanggang@uestc.edu.cn, 2015010913035@std.uestc.edu.cn).

Y.-C. Liang is with the Center for Intelligent Networking and Communications (CINC), University of Electronic Science and Technology of China (UESTC), Chengdu 611731, China (e-mail: liangyc@ieee.org). (*Corresponding author: Y.-C. Liang.*)

O. Tirkkonen is with the Aalto University, Aalto, Finland. (e-mail:olav.tirkkonen@aalto.fi)

I. INTRODUCTION

A. Motivation

Device-to-device (D2D) communication underlying a cellular network, which allows a device to communicate with its proximity device over the licensed cellular bandwidth, is recognized as a promising wireless technology [1] and a competitive candidate for evolved/beyond 5th-Generation (5G) system standards [2]. Specifically, the overall network's spectrum efficiency (SE) can be enhanced, since additional D2D links are supported by sharing the licensed cellular spectrums; the overall network's energy efficiency (EE) can be improved by exploiting the proximity of D2D users; also, the transmission delay can be reduced by eliminating the forwarding through a cellular base station (BS). However, interference management is one of the most important challenges for underlying D2D communication [1]–[3]. The D2D link and the cellular link operating in the same licensed band interfere with each other severely [4], and the interference needs to be carefully suppressed via efficient interference control [5] [6] and resource allocation [7] [8]. Existing interference management schemes were designed under the fact that wireless environment including interference channels is fixed. Thus the extent of interference suppression is fundamentally limited.

Recently, reconfigurable intelligent surface (RIS) has emerged as a new and revolutionary technology to achieve spectrum-, energy- and cost-efficient wireless networks [9]–[11]. An RIS consists of a large number of passive low-cost reflecting elements, each of which can adjust the phase and amplitude of the incident electromagnetic wave in a software-defined way and reflect it passively [12]. Thus, RIS is able to enhance desired signals and suppress interference by designing passive beamforming (i.e., changing each reflecting element's reflecting coefficient including amplitude and phase). In particular, a typical architecture of RIS consists of a smart controller and three layers (i.e., reflecting element, copper backplane, and control circuit board) [9]. The controller attached to RIS can intelligently adjust the reflecting coefficients and communicate with other network components. Hence, it is realizable to intentionally reconfigure the wireless propagation environment and thus fundamentally improve the interference management level for underlying D2D communication.

RIS can be explored to not only suppress the severe interference between each paired D2D link and cellular link, but also enhance the strength of desired signals for both D2D links and cellular links. This motivates us to study RIS-empowered D2D communication underlying a cellular network as shown in Fig. 1, which consists of multiple D2D pairs and multiple cellular users (CUs), as well as an RIS. This has not been studied in the literature to our best knowledge.

B. Related Works

1) *D2D Communication*: D2D communication systems have been widely studied in [13]–[24]. Thereinto, interference management and performance analysis were investigated in [13]–[20]. For both direct D2D communication network and D2D communication underlying cellular networks, the throughput over the shared resources was maximized in [13] by optimizing the resource allocation under the quality-of-service (QoS) requirements for both D2D users and CUs. For D2D communication underlying cellular networks, the overall network's SE was maximized in [14] by jointly optimizing the resource reuse indicators and transmit power. For D2D communication underlying an orthogonal-frequency-division-multiplexing (OFDM) cellular network, the average ergodic sum rate over D2D pairs' locations was maximized in [15] by jointly optimizing the subcarrier assignment and power allocation. For D2D communication underlying a multiuser multiple-input multiple-output (MU-MIMO) cellular network, the total transmit power of the overall network was minimized in [16], by jointly optimizing the BS's transmit beamforming and the transmit power of both BS and D2D transmitters. For a direct D2D communication network, a deep learning approach was proposed in [17] to maximize the overall network's SE by optimizing the scheduling of D2D links. The overall EE of an underlying D2D network, which allows multiple D2D users pair with a CU, was maximized in [18] by jointly optimizing the resource reuse indicators and power allocation. The overall EE was maximized in [19] for dedicated transmission mode, reusing transmission mode and cellular transmission mode, while considering the circuit power consumption and the QoS requirements for D2D users and CUs. The performance of an underlying D2D network over fading channels was analyzed in [20] by leveraging a stochastic geometric approach.

D2D communication has also been incorporated with other advanced wireless communication technologies. For example, a two-phase cooperative transmission scheme was proposed in [21] for D2D communication underlying cellular networks, in which the policy of dynamic precoding and power allocation was designed. For full-duplex D2D underlying cellular networks, two cooperative modes based on network MU-MIMO and sequential forwarding, respectively, were proposed in [23] to achieve both proximity gain and resource-reuse gain. The coverage and rate performance of UAV communication with underlying D2D users were investigated in [24].

2) *Wireless Communication with RIS*: Wireless communication systems with RIS can be divided into two categories, i.e., RIS-based transceiver design and RIS-assisted wireless communication. For the former, the RISs are utilized as transmit antennas and receive antennas to significantly reduce

the hardware cost of traditional wireless transceivers [25]. Most literature were under the latter category, in which RIS is applied to improve the performance of wireless systems. RIS resembles but differs from existing technologies like full-duplex amplify-and-forward (AF) relaying and backscatter communications. A full-duplex AF relay actively processes the received signals and transmits the amplified signals, introducing additional noise and several interference at the relay; while an RIS passively reflects the signals instead of amplification, thus it avoids consuming power for active transmission and no noise or self-interference is introduced [26]. Backscatter communication enables a tag to deliver its own information to a receiver by intentionally switching the antenna's load impedances [27] [28], while an RIS is used to enhance the existing communication link performance.

RIS-assisted wireless communication was extensively studied in the prior works. For example, the weighted sum rate of an RIS-aided multiuser multiple-input single-output (MISO) downlink system was maximized in [29], by jointly optimizing the BS's active beamforming and the RIS's passive beamforming (i.e., reflecting coefficients). The ergodic sum rate of an RIS-assisted MISO system was maximized in [30] through deep reinforcement learning, by jointly optimizing the BS's transmit beamforming and the RIS's phase shifts. In [31], the distribution of SE was asymptotically analyzed and the reliability was verified for an RIS-empowered uplink system. For an RIS-assisted downlink non-orthogonal-multiple-access system, the max-min rate performance was optimized in [32]. The EE of an RIS-empowered downlink multiuser system was maximized in [33], by jointly optimizing the BS's transmit power and the RIS's passive beamforming. The minimum secrecy rate of an RIS-assisted MISO system was maximized in [34].

C. Contributions

In this paper, we study the resource allocation for an RIS-empowered underlying D2D communication network as shown in Fig. 1. This work is an extension of the conference-version paper [35]. The main contributions are summarized as follows

- We formulate a problem to maximize the overall network's SE (i.e., sum rate of both D2D users and CUs), by jointly optimizing the resource reuse indicators (i.e., user pairing between D2D users and CUs), the transmit power and the RIS's passive beamforming, subject to the signal-to-interference-plus-noise ratio (SINR) constraints for both D2D links and cellular links as well as other practical constraints. However, the problem is challenging to be solved optimally, since the user pairing (involving integer variables) and the resource allocation are closely coupled.

- To decouple the SE-maximization problem, we first propose an efficient relative-channel-strength (RCS) based user-pairing scheme with low complexity. Under the obtained user-pairing design, an iterative algorithm based on alternating optimization (AO) is further proposed. Specifically, for given passive beamforming, the successive convex approximation (SCA) is exploited to optimize the transmit power; while for given transmit power, the Lagrangian dual transform and quadratic transform are exploited to solve the resulting multiple-ratio fractional programming problem. The algorithm's convergence and complexity are also analyzed.
- Based on the proposed model of RIS power consumption, we formulate a problem to maximize the overall network's EE, by jointly optimizing the resource reuse indicators, the transmit power and the RIS's passive beamforming, subject to the same constraints as the SE-maximization problem. To solve this non-convex problem, the proposed RCS based user-pairing scheme is first utilized to determine the resource reuse indicators, and an AO-based algorithm integrated with Dinkelbach's method is then proposed to optimize the transmit power and RIS's passive beamforming iteratively. The algorithms's convergence and complexity are also analyzed.
- Numerical results show that the proposed design achieves significant SE and EE enhancements compared to traditional underlying D2D without RIS, and suffers from slight degradation compared to the best-achievable performance under ideal user pairing. A 2-bit quantized phase shifter achieves sufficient SE enhancement compared to the ideal case of continuous phase shifter, and the highest EE for practical cases of finite-resolution phase shifter. The effects of main parameters on the performances are numerically verified, such as number of reflecting elements and CUs, and CUs' minimum rate requirement.

D. Organization and Notations

The rest of this paper is organized as follows. Section II presents the system model for RIS-empowered underlying D2D communication network. Section III formulates the SE maximization problem. Section IV proposes an RCS based user-pairing scheme and an efficient iterative algorithm to solve the SE-maximization problem. Section V formulates and solves the EE-maximization problem. Section VI provides numerical results. Section VII concludes this paper.

The main notations are as follows. Denote scalars, vectors and matrices by italic letters, bold-face lower-case letters and bold-face upper-case letters, respectively, e.g., a , \mathbf{a} , \mathbf{A} . Denote the space of $x \times y$ complex matrices by $\mathcal{C}^{x \times y}$. Denote the set of real number and positive real number by \mathcal{R}

and \mathcal{R}^+ , respectively. Denote the distribution of a circularly symmetric complex Gaussian (CSCG) random variable with mean μ and variance σ^2 by $\mathcal{CN}(\mu, \sigma^2)$. Denote the transpose and conjugate transpose of a vector \mathbf{v} by \mathbf{v}^T and \mathbf{v}^H , respectively. Denote the operation of taking real part by $\text{Re}\{\cdot\}$.

II. SYSTEM MODEL

In this section, we first describe the RIS-empowered underlying D2D communication network, and then present the signal model.

A. System Description

As shown in Fig. 1, we consider an RIS-empowered cellular network with underlay D2D, which consists of an RIS, N ($N \geq 1$) D2D transmitters (TXs) denoted as TX 1, ..., TX N , N D2D receivers (RXs) denoted as RX 1, ..., RX N , K ($K \geq 1$) active CUs (i.e., cellular users) denoted as CU 1, ..., CU K , and a cellular BS. The RIS has M ($M \geq 1$) reflecting elements, while each D2D TX, D2D RX, CU and the BS are equipped with a single antenna. A controller is attached to the RIS to control the reflecting coefficients and communicate with other network components through separate wireless links. We assume that the D2D links share the uplink (UL) spectrum of the cellular network, since the UL spectrum is typically underutilized compared to the downlink spectrum. To alleviate interference, we further assume that a D2D link shares at most one CU's spectrum resource, while the resource of a CU can be shared by at most one D2D link [14] [36].

All channels are assumed to experience quasi-static flat fading. The channels from TX i ($1 \leq i \leq N$) to RX l ($1 \leq l \leq N$) and RIS are denoted by $h_{l,i} \in \mathcal{C}$ and $\mathbf{f}_i \in \mathcal{C}^{M \times 1}$, respectively. For notational clarity, we represent each channel related to the cellular network with a tilde. The channels from CU k ($1 \leq k \leq K$) to BS and RIS are denoted by $\tilde{h}_k \in \mathcal{C}$ and $\tilde{\mathbf{f}}_k \in \mathcal{C}^{M \times 1}$, respectively; the channels from RIS to RX l and BS are denoted by $\mathbf{g}_l \in \mathcal{C}^{M \times 1}$ and $\tilde{\mathbf{g}} \in \mathcal{C}^{M \times 1}$, respectively; the interference channels from TX i to BS and from CU k to RX l are denoted by $u_i \in \mathcal{C}$ and $v_{l,k} \in \mathcal{C}$, respectively.

B. Signal Model

Let $\Phi = \text{diag}\{\alpha_1 e^{j\theta_1}, \dots, \alpha_M e^{j\theta_M}\} \in \mathcal{C}^{M \times M}$ denote the reflecting coefficient matrix of the RIS, where $\alpha_m \in \mathcal{R}^+$ and $\theta_m \in \mathcal{R}$ denote the reflecting amplitude and reflecting phase shift of the m -th reflecting element, for $1 \leq m \leq M$, respectively. Let $\beta_m = \alpha_m e^{j\theta_m} \in \mathcal{F}$ denote the reflecting

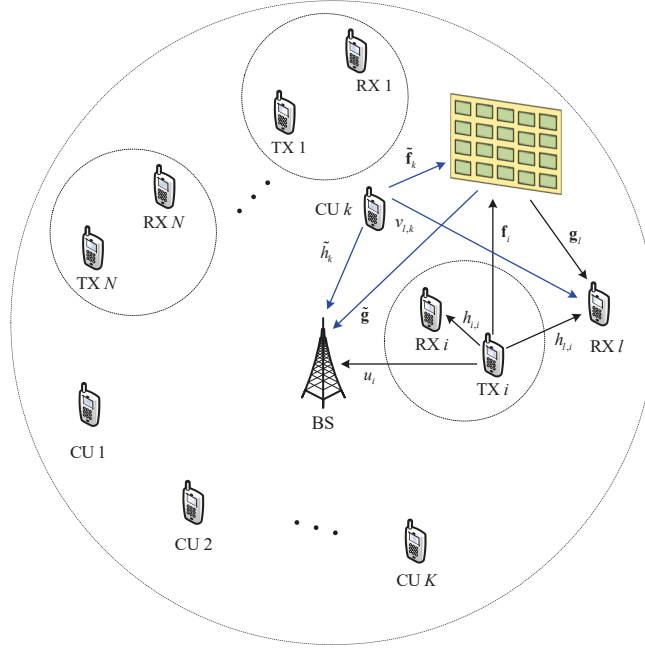


Fig. 1: An RIS-empowered underlaying D2D communication network.

coefficient, where \mathcal{F} is the feasible set of the reflecting coefficients. Three different settings for reflecting coefficients are considered in this paper.

1) *Ideal Reflecting Coefficients*: The amplitude and phase of each reflecting element are continuously adjustable. Specifically, the reflecting amplitude $\alpha_m \in [0, 1]$, and the reflecting phase shift $\theta_m \in [0, 2\pi)$. The set of all reflecting coefficients with ideal reflecting coefficient is

$$\mathcal{F}_1 = \left\{ \beta_m = \alpha_m e^{j\theta_m} \mid |\beta_m|^2 \leq 1 \right\}. \quad (1)$$

2) *Continuous Reflecting Phase Shift*: The reflecting phase shift θ_m takes continuous values in the range $[0, 2\pi)$, while the reflecting amplitude α_m takes the maximum value of 1. The set of reflecting coefficients with continuous reflecting phase shift is

$$\mathcal{F}_2 = \left\{ \beta_m = e^{j\theta_m} \mid \theta_m \in [0, 2\pi) \right\}. \quad (2)$$

3) *Discrete Reflecting Phase Shift*: In this setting, $\alpha_m = 1$, and the reflecting phase shift θ_m is B -bit quantized, taking 2^B discrete values. The corresponding set of reflecting coefficients is

$$\mathcal{F}_3 = \left\{ \beta_m = e^{j\theta_m} \mid \theta_m \in \left\{ 0, \frac{2\pi}{2^B}, \dots, \frac{2\pi(2^B - 1)}{2^B} \right\} \right\}. \quad (3)$$

From [10] [11], different reflecting amplitudes and phase shifts can be realized by switching

different resistor loads and setting different bias voltages to tuning elements that are typically varactor diodes, respectively. Due to hardware characteristic and cost limitations, it is practical to achieve finite-resolution phase shift. Therefore, the set of discrete reflecting phase shifts \mathcal{F}_3 is in common use. Nevertheless, it is important to evaluate the system performances with \mathcal{F}_1 and \mathcal{F}_2 , which provide upper bounds for the performance with \mathcal{F}_3 .

The transmit signals from TX i and CU k are denoted as s_i and x_k , respectively, which follow independent CSCG distribution with zero mean and unit variance, i.e., $s_i \sim \mathcal{CN}(0, 1)$, $x_k \sim \mathcal{CN}(0, 1)$. Denote the index set of active D2D pairs as $\mathcal{D} \subseteq \{1, \dots, N\}$. The corresponding SINR for RX n decoding s_n from D2D TX $n \in \mathcal{D}$ is

$$\gamma_n^d = \frac{P_n^d |\mathbf{g}_n^H \Phi \mathbf{f}_n + h_{n,n}|^2}{\sum_{k=1}^K \rho_{k,n} P_k^c |\mathbf{g}_n^H \Phi \tilde{\mathbf{f}}_k + v_{n,k}|^2 + \sigma^2}, \quad (4)$$

where P_i^d and P_k^c are the transmit power of TX i and CU k , respectively; $\rho_{k,n}$ is the resource reuse indicator for cellular link k and D2D link n , $\rho_{k,n} = 1$ when D2D link n reuses the resource of CU k , and $\rho_{k,n} = 0$ otherwise; σ^2 is the power of additive white Gaussian noise (AWGN) at RX n .

The SINR for the BS decoding x_k from CU k is

$$\gamma_k^c = \frac{P_k^c |\tilde{\mathbf{g}}^H \Phi \tilde{\mathbf{f}}_k + \tilde{h}_k|^2}{\sum_{i=1}^N \rho_{k,i} P_i^d |\tilde{\mathbf{g}}^H \Phi \mathbf{f}_i + u_i|^2 + \sigma^2}, \quad (5)$$

where σ^2 is the power of AWGN at the BS.

Hence, the overall network's SE (i.e., sum rate of both D2D users and CUs) in bps/Hz is

$$R(\boldsymbol{\rho}, \mathbf{p}, \Phi) = \sum_{n \in \mathcal{D}} \log_2(1 + \gamma_n^d) + \sum_{k=1}^K \log_2(1 + \gamma_k^c), \quad (6)$$

where the length- (KN) resource reuse indicator vector $\boldsymbol{\rho} = [\rho_{1,1}, \dots, \rho_{1,N}, \rho_{2,1}, \dots, \rho_{K,N}]^T$, and the length- $(K + N)$ power allocation vector $\mathbf{p} = [P_1^d, \dots, P_N^d, P_1^c, \dots, P_K^c]^T$.

III. PROBLEM FORMULATION FOR SE MAXIMIZATION

In this section, we formulate a problem to maximize the SE in (6), by jointly optimizing the resource reuse indicator vector $\boldsymbol{\rho}$, the transmit power vector \mathbf{p} and the reflecting coefficients matrix

Φ . The optimization problem is formulated as follows

$$(P1) : \max_{\boldsymbol{\rho}, \mathbf{p}, \Phi} R(\boldsymbol{\rho}, \mathbf{p}, \Phi) \quad (7a)$$

$$\text{s.t. } \gamma_n^d \geq \gamma_{\min}^d, \quad n \in \mathcal{D} \quad (7b)$$

$$\gamma_k^c \geq \gamma_{\min}^c, \quad 1 \leq k \leq K \quad (7c)$$

$$\sum_{k=1}^K \rho_{k,n} \leq 1 \quad (7d)$$

$$\sum_{n \in \mathcal{D}} \rho_{k,n} \leq 1 \quad (7e)$$

$$0 \leq P_n^d \leq P_{\max}^d \quad (7f)$$

$$0 \leq P_k^c \leq P_{\max}^c \quad (7g)$$

$$\beta_m \in \mathcal{F}, \quad 1 \leq m \leq M \quad (7h)$$

where (7b) and (7c) indicate the required minimum SINRs (i.e., QoS) γ_{\min}^d and γ_{\min}^c for D2D links and cellular links, respectively; (7d) ensures that a D2D link shares at most one CU's resource, while (7e) indicates that the resource of a CU can be shared by at most one D2D link; (7f) and (7g) are the maximum transmit power constraints on the TXs and CUs, respectively; and (7h) is the practical constraint on the reflecting coefficients with $\mathcal{F} \in \{\mathcal{F}_1, \mathcal{F}_2, \mathcal{F}_3\}$.

Notice that (P1) is a non-convex problem. First, (P1) involves integer variables $\boldsymbol{\rho}$ and thus is NP-hard. Moreover, the objective function and the constraint functions of (7b) and (7c) are non-concave with respect to the variables $\boldsymbol{\rho}$, \mathbf{p} and Φ , and these variables are all coupled. There is no standard method to solve such a non-convex problem. In the sequel, we first propose an user-pairing scheme with low complexity to determine the value of the resource reuse indicator vector $\boldsymbol{\rho}$. Then, we propose an efficient algorithm based on the AO (i.e., alternating optimization), SCA (i.e., successive convex approximation), Lagrangian dual transform and quadratic transform techniques to optimize \mathbf{p} and Φ in an iterative manner.

IV. SOLUTION TO SE-MAXIMIZATION PROBLEM

In order to solve the SE-Maximization problem (P1), we first propose an efficient user-pairing scheme to determine integer variables $\boldsymbol{\rho}$, then optimize \mathbf{p} and Φ in an iterative manner. To begin with, we solve (P1) with $\mathcal{F} = \mathcal{F}_1$, which makes (7h) a convex constraint. Therefore, the non-convexity

of (P1) only roots from the objective function and other constraints. Afterwards, we utilize the projection method to obtain heuristic solutions to (P1) with $\mathcal{F} = \mathcal{F}_2$ and $\mathcal{F} = \mathcal{F}_3$.

A. Relative-Channel-Strength based Pairing Scheme

Since the user-pairing design involves integer programming which is hard to solve, we propose a relative-channel-strength (RCS) based low-complexity pairing scheme to design the resource reuse indicators ρ .

Notice that there are A_K^N different possible pairings denoted as a set $\Pi \triangleq \{\pi_1, \dots, \pi_{A_K^N}\}$. Each possible pairing can be viewed as an index mapping denoted as $\pi_q : k \in \mathcal{U}_q \rightarrow n \in \mathcal{D}_q$, for $q = 1, \dots, A_K^N$, i.e., the π_q maps each CU index $k \in \mathcal{U}_q \subset \{1, 2, \dots, K\}$ to a D2D-link index $n \in \mathcal{D}_q \subset \mathcal{D}$. The RCS-based pairing scheme determines the pairing π_{q^*} by the following criterion

$$\pi_{q^*} = \arg \max_{\pi_q \in \Pi} \sum_{k \in \mathcal{U}_q} \frac{|\tilde{h}_k|^2}{|v_{\pi_q(k), k}|^2} + \frac{|h_{\pi_q(k), \pi_q(k)}|^2}{|u_{\pi_q(k)}|^2}. \quad (8)$$

This heuristic pairing scheme chooses the pairing mapping which maximizes the sum of the relative channels that is defined as the ratio of (transmitter-to-receiver) useful channel strength over interference channel strength. Specifically, the first term in the summation of (8) is the ratio of each paired CU-to-BS channel strength over the paired CU-to-RX interference channel strength, and the second term is the ratio of each paired TX-to-RX channel strength over the paired TX-to-BS interference channel strength.

Clearly, this heuristic pairing scheme that requires only simple comparison features low complexity, but fortunately its resultant design only suffers from slight performance degradation compared to the design with ideal pairing achieved by exhaustive search, as numerically shown in Section VI. This RCS-based pairing scheme will also be used for EE maximization in Section V.

B. Optimize Transmit Power Vector \mathbf{p}

In each iteration j , for given reflecting coefficient matrix $\Phi^{(j)}$, the transmit power vector \mathbf{p} can be optimized by solving the following subproblem

$$(P1.1) : \quad \max_{\mathbf{p}} \quad R(\mathbf{p}) \quad (9a)$$

$$\text{s.t.} \quad (7b), (7c), (7f), (7g). \quad (9b)$$

Since the objective function of (P1.1) is not concave with respect to the optimization variable \mathbf{p} , (P1.1) is non-convex. Notice that the objective function can be rewritten as follows

$$R = \sum_{n \in \mathcal{D}} \left[\log_2 (P_n^d Q_{n,n}^{(j)} + A_1) - \log_2 (A_1) \right] + \sum_{k=1}^K \left[\log_2 (P_k^c Q_k^{(j)} + A_2) - \log_2 (A_2) \right], \quad (10)$$

where $Q_{n,n} = |\mathbf{g}_n^H \Phi \mathbf{f}_n + h_{n,n}|^2$, $\tilde{Q}_{n,k} = |\mathbf{g}_n^H \Phi \tilde{\mathbf{f}}_k + v_{n,k}|^2$, $\tilde{Q}_k = |\tilde{\mathbf{g}}^H \Phi \tilde{\mathbf{f}}_k + \tilde{h}_k|^2$, $Q_i = |\tilde{\mathbf{g}}^H \Phi \mathbf{f}_i + u_i|^2$, $A_1 = \sum_{k=1}^K \rho_{k,n} P_k^c \tilde{Q}_{n,k}^{(j)} + \sigma^2$ and $A_2 = \sum_{i=1}^N \rho_{k,i} P_i^d Q_i^{(j)} + \sigma^2$.

The non-convexity of (10) comes from the items $-\log_2(A_1)$ and $-\log_2(A_2)$. We exploit the SCA technique [37] to solve (P1.1). Specifically, we need to find a concave lower bound to approximate the objective function. From the fact that any convex function can be lower bounded by its first-order Taylor expansion at any point, we obtain the following concave lower bound R^{lb} at the local point $\mathbf{p}^{(j)}$

$$R \geq \sum_{n \in \mathcal{D}} \left[\log_2 (P_n^d Q_{n,n}^{(j)} + A_1) - \log_2 (A_1^{(j)}) - \frac{1}{A_1^{(j)}} \sum_{k=1}^K \rho_{k,n} \tilde{Q}_{n,k}^{(j)} (P_k^c - P_k^{c(j)}) \right] \\ + \sum_{k=1}^K \left[\log_2 (P_k^c \tilde{Q}_k^{(j)} + A_2) - \log_2 (A_2^{(j)}) - \frac{1}{A_2^{(j)}} \sum_{i=1}^N \rho_{k,i} Q_i^{(j)} (P_i^d - P_i^{d(j)}) \right] \triangleq R^{\text{lb}}. \quad (11)$$

With given local point $\mathbf{p}^{(j)}$ and lower bound R^{lb} , the subproblem (P1.1) is approximated as

$$\text{(P1.1.A)} : \max_{\mathbf{p}} R^{\text{lb}} \quad (12a)$$

$$\text{s.t. (7b), (7c), (7f), (7g).} \quad (12b)$$

Problem (P1.1.A) is a convex problem which can be efficiently solved with standard toolbox, e.g., CVX [38]. Notice that the adopted lower bound R^{lb} implies that the feasible set of (P1.1.A) is always a subset of that of (P1.1). As a result, the optimal objective value obtained from (P1.1.A) is in general a lower bound to that of (P1.1).

C. Optimize Reflecting Coefficient Matrix with $\mathcal{F} = \mathcal{F}_1$

In each iteration j , for given transmit power vector $\mathbf{p}^{(j)}$, the reflecting coefficient matrix Φ can be optimized by solving the following subproblem

$$\text{(P1.2)} : \max_{\Phi} R(\Phi) \quad (13a)$$

$$\text{s.t. (7b), (7c), (7h).} \quad (13b)$$

The logarithm in the objective function makes it difficult to solve (P1.2). Therefore, we tackle it via the Lagrangian dual transform proposed in [39]. Introducing auxiliary variables $\boldsymbol{\eta}^d = [\eta_1^d, \dots, \eta_N^d]^T$ and $\boldsymbol{\eta}^c = [\eta_1^c, \dots, \eta_K^c]^T$, the subproblem (P1.2) can be equivalently reformulated as

$$\text{(P1.2.L): } \max_{\Phi} R_a(\Phi) \quad (14a)$$

$$\text{s.t. (7b), (7c), (7h),} \quad (14b)$$

where the new objective function $R_a(\Phi)$ is expressed as

$$\begin{aligned} R_a(\Phi) = & \max_{\eta_n^d} \left(\sum_{n \in \mathcal{D}} \log(1 + \eta_n^d) - \sum_{n \in \mathcal{D}} \eta_n^d + \sum_{n \in \mathcal{D}} \frac{(1 + \eta_n^d)\gamma_n^d}{1 + \gamma_n^d} \right) \\ & + \max_{\eta_k^c} \left(\sum_{k=1}^K \log(1 + \eta_k^c) - \sum_{k=1}^K \eta_k^c + \sum_{k=1}^K \frac{(1 + \eta_k^c)\gamma_k^c}{1 + \gamma_k^c} \right). \end{aligned} \quad (15)$$

Actually, we first optimize η_n^d and η_k^c with fixed γ_n^d and γ_k^c , respectively; then optimize γ_n^d and γ_k^c with fixed η_n^d and η_k^c , respectively. It can be easily checked that R_a is a concave differentiable function over η_n^d with γ_n^d being fixed, so the optimal value of η_n^d can be obtained by setting $\partial R_a(\gamma_n^{d(j)})/\partial \eta_n^d = 0$, i.e., $\eta_{\text{opt},n}^{d(j)} = \gamma_n^{d(j)}$. Similarly, $\eta_{\text{opt},k}^{c(j)} = \gamma_k^{c(j)}$. Replacing η_n^d and η_k^c with $\eta_{\text{opt},n}^{d(j)}$ and $\eta_{\text{opt},k}^{c(j)}$, respectively, we find that the optimal objective values of (P1.2) and (P1.2.L) are equal, i.e., $R_a = R$.

Then, with given optimal $\eta_{\text{opt}}^{d(j)}$ and $\eta_{\text{opt}}^{c(j)}$, (P1.2.L) is transformed into

$$\text{(P1.2.E): } \max_{\Phi} R_b(\Phi) \quad (16a)$$

$$\text{s.t. (7b), (7c), (7h),} \quad (16b)$$

where $R_b(\Phi)$ is expressed as

$$R_b(\Phi) = \sum_{n \in \mathcal{D}} \frac{(1 + \eta_{\text{opt},n}^{d(j)})\gamma_n^d}{1 + \gamma_n^d} + \sum_{k=1}^K \frac{(1 + \eta_{\text{opt},k}^{c(j)})\gamma_k^c}{1 + \gamma_k^c}. \quad (17)$$

Further, we define $\boldsymbol{\theta}^H \boldsymbol{\omega}_{n,n} = \mathbf{g}_n^H \Phi \mathbf{f}_n$, $\boldsymbol{\theta}^H \tilde{\boldsymbol{\omega}}_{n,k} = \mathbf{g}_n^H \Phi \tilde{\mathbf{f}}_k$, $\boldsymbol{\theta}^H \tilde{\boldsymbol{\omega}}_k = \tilde{\mathbf{g}}^H \Phi \tilde{\mathbf{f}}_k$ and $\boldsymbol{\theta}^H \boldsymbol{\omega}_i = \tilde{\mathbf{g}}^H \Phi \mathbf{f}_i$. From (4) and (5), optimizing the reflecting coefficient matrix Φ can be equivalently transformed

into optimizing $\boldsymbol{\theta}$ in the following objective function

$$R_b(\boldsymbol{\theta}) = \sum_{n \in \mathcal{D}} \frac{\left(1 + \eta_{\text{opt},n}^{d(j)}\right) P_n^{d(j)} Q_{n,n}^w}{P_n^{d(j)} Q_{n,n}^w + \sum_{k=1}^K \rho_{k,n} P_k^{c(j)} \tilde{Q}_{n,k}^w + \sigma^2} + \sum_{k=1}^K \frac{\left(1 + \eta_{\text{opt},k}^{c(j)}\right) P_k^{c(j)} \tilde{Q}_k^w}{P_k^{c(j)} \tilde{Q}_k^w + \sum_{i=1}^N \rho_{k,i} P_i^{d(j)} Q_i^w + \sigma^2}, \quad (18)$$

where $Q_{n,n}^w = |\boldsymbol{\theta}^H \boldsymbol{\omega}_{n,n} + h_{n,n}|^2$, $\tilde{Q}_{n,k}^w = |\boldsymbol{\theta}^H \tilde{\boldsymbol{\omega}}_{n,k} + v_{n,k}|^2$, $\tilde{Q}_k^w = |\boldsymbol{\theta}^H \tilde{\boldsymbol{\omega}}_k + \tilde{h}_k|^2$ and $Q_i^w = |\boldsymbol{\theta}^H \boldsymbol{\omega}_i + u_i|^2$.

Actually, (P1.2.E) can be equivalently reformulated as follows

$$\text{(P1.2.T)} : \max_{\boldsymbol{\theta}} R_b(\boldsymbol{\theta}) \quad (19a)$$

$$\text{s.t. (7b), (7c), (7h).} \quad (19b)$$

Problem (P1.2.T) is a multiple-ratio fractional programming problem, which can be solved by utilizing the quadratic transform technique proposed in [39]. Introducing auxiliary variable $\mathbf{y} = [y_1^d, \dots, y_N^d, y_1^c, \dots, y_K^c]^T$, the objective function of (P1.2.T) can be transformed as follows

$$R_b(\boldsymbol{\theta}, \mathbf{y}) = \sum_{n \in \mathcal{D}} \left[2\sqrt{\left(1 + \eta_{\text{opt},n}^{d(j)}\right) P_n^{d(j)}} \text{Re} \left\{ y_n^{d*} \boldsymbol{\theta}^H \boldsymbol{\omega}_{n,n} + y_n^{d*} h_{n,n} \right\} - |y_n^d|^2 \left(P_n^{d(j)} Q_{n,n}^w + \sum_{k=1}^K \rho_{k,n} P_k^{c(j)} \tilde{Q}_{n,k}^w + \sigma^2 \right) \right] + \sum_{k=1}^K \left[2\sqrt{\left(1 + \eta_{\text{opt},k}^{c(j)}\right) P_k^{c(j)}} \text{Re} \left\{ y_k^{c*} \boldsymbol{\theta}^H \tilde{\boldsymbol{\omega}}_k + y_k^{c*} \tilde{h}_k \right\} - |y_k^c|^2 \left(P_k^{c(j)} \tilde{Q}_k^w + \sum_{i=1}^N \rho_{k,i} P_i^{d(j)} Q_i^w + \sigma^2 \right) \right]. \quad (20)$$

Similarly, we first optimize \mathbf{y} with fixed $\boldsymbol{\theta}$, then optimize $\boldsymbol{\theta}$ with fixed \mathbf{y} . It can be easily checked that $R_b(\boldsymbol{\theta}, \mathbf{y})$ is a concave differentiable function over \mathbf{y} with fixed $\boldsymbol{\theta}$, so the optimal solution of \mathbf{y} can be obtained by setting $\partial R_b(\mathbf{y}, \boldsymbol{\theta}^{(j)}) / \partial \mathbf{y} = 0$. Thus, the optimal value of \mathbf{y} is given by

$$y_{\text{opt},n}^{d(j)} = \frac{\sqrt{\left(1 + \eta_{\text{opt},n}^{d(j)}\right) P_n^{d(j)}} \left[\boldsymbol{\theta}^{H(j)} \boldsymbol{\omega}_{n,n} + h_{n,n} \right]}{P_n^{d(j)} Q_{n,n}^w + \sum_{k=1}^K \rho_{k,n} P_k^{c(j)} \tilde{Q}_{n,k}^w + \sigma^2}, \quad (21)$$

$$y_{\text{opt},n}^{c(j)} = \frac{\sqrt{\left(1 + \eta_{\text{opt},k}^{c(j)}\right) P_k^{c(j)}} \left[\boldsymbol{\theta}^{H(j)} \tilde{\boldsymbol{\omega}}_k + \tilde{h}_k \right]}{P_k^{c(j)} \tilde{Q}_k^w + \sum_{i=1}^N \rho_{k,i} P_i^{d(j)} Q_i^w + \sigma^2}. \quad (22)$$

Then, we optimize $\boldsymbol{\theta}$ for given \mathbf{y} . Replacing $y_n^{d(j)}$ and $y_k^{c(j)}$ with $y_{\text{opt},n}^{d(j)}$ and $y_{\text{opt},k}^{c(j)}$, respectively. De-

note $\mathbf{B}_{1n} = P_n^{d(j)} \boldsymbol{\omega}_{n,n} \boldsymbol{\omega}_{n,n}^H$, $\mathbf{B}_{2n} = \sum_{k=1}^K \rho_{k,n} P_k^{c(j)} \tilde{\boldsymbol{\omega}}_{n,k} \tilde{\boldsymbol{\omega}}_{n,k}^H$, $\mathbf{B}_{1b} = P_k^{c(j)} \tilde{\boldsymbol{\omega}}_k \tilde{\boldsymbol{\omega}}_k^H$, $\mathbf{B}_{2b} = \sum_{i=1}^N \rho_{k,i} P_i^{d(j)} \boldsymbol{\omega}_i \boldsymbol{\omega}_i^H$, $\mathbf{e}_{1n} = P_n^{d(j)} h_{n,n}^* \boldsymbol{\omega}_{n,n}$, $\mathbf{e}_{2n} = \sum_{k=1}^K \rho_{k,n} P_k^{c(j)} v_{n,k}^* \tilde{\boldsymbol{\omega}}_{n,k}$, $\mathbf{e}_{1b} = P_k^{c(j)} \tilde{h}_k^* \tilde{\boldsymbol{\omega}}_k$ and $\mathbf{e}_{2b} = \sum_{i=1}^N \rho_{k,i} P_i^{d(j)} u_i^* \boldsymbol{\omega}_i$.

Notice that the term $|\boldsymbol{\theta}^H \boldsymbol{\omega} + h|^2$ can be expanded as follows

$$|\boldsymbol{\theta}^H \boldsymbol{\omega} + h|^2 = \boldsymbol{\theta}^H \boldsymbol{\omega} \boldsymbol{\omega}^H \boldsymbol{\theta} + 2\text{Re}(\boldsymbol{\theta}^H \boldsymbol{\omega} h^*) + |h|^2. \quad (23)$$

For given \mathbf{y} , the objective function is transformed as follows

$$R_b(\boldsymbol{\theta}, \mathbf{y}) = -\boldsymbol{\theta}^H \mathbf{B}_1 \boldsymbol{\theta} + 2\text{Re}(\boldsymbol{\theta}^H \mathbf{e}_1) + C_1, \quad (24)$$

where C_1 is a constant, the matrix \mathbf{B}_1 and vector \mathbf{e}_1 are

$$\begin{aligned} \mathbf{B}_1 &= \sum_{n \in \mathcal{D}} \left| y_{\text{opt},n}^{d(j)} \right|^2 \mathbf{B}_n + \sum_{k=1}^K \left| y_{\text{opt},k}^{c(j)} \right|^2 \mathbf{B}_b \\ \mathbf{e}_1 &= \sum_{n \in \mathcal{D}} \left[\sqrt{\left(1 + \eta_{\text{opt},n}^{d(j)}\right)} P_n^{d(j)} \left(y_{\text{opt},n}^{d(j)} \right)^* \boldsymbol{\omega}_{n,n} - \left| y_{\text{opt},n}^{d(j)} \right|^2 \mathbf{e}_n \right] + \sum_{k=1}^K \left[\sqrt{\left(1 + \eta_{\text{opt},k}^{c(j)}\right)} P_k^{c(j)} \left(y_{\text{opt},k}^{c(j)} \right)^* \tilde{\boldsymbol{\omega}}_k - \left| y_{\text{opt},k}^{c(j)} \right|^2 \mathbf{e}_b \right], \end{aligned} \quad (25)$$

$$(26)$$

with $\mathbf{B}_n = \mathbf{B}_{1n} + \mathbf{B}_{2n}$, $\mathbf{B}_b = \mathbf{B}_{1b} + \mathbf{B}_{2b}$, $\mathbf{e}_n = \mathbf{e}_{1n} + \mathbf{e}_{2n}$, and $\mathbf{e}_b = \mathbf{e}_{1b} + \mathbf{e}_{2b}$.

Similarly, introducing an auxiliary variable x_d , the constraint function of (7b) can be equivalently written as

$$f_d(\boldsymbol{\theta}, x_d) = 2\sqrt{P_n^{d(j)}} \text{Re} \left(x_d^* \boldsymbol{\theta}^H \boldsymbol{\omega}_{n,n} + x_d^* h_{n,n} \right) - |x_d|^2 \left(\sum_{k=1}^K \rho_{k,n} P_k^{c(j)} \tilde{Q}_{n,k}^w + \sigma^2 \right). \quad (27)$$

Introducing an auxiliary variable x_c , the constraint function of (7c) can be equivalently written as follows

$$f_c(\boldsymbol{\theta}, x_c) = 2\sqrt{P_k^{c(j)}} \text{Re} \left(x_c^* \boldsymbol{\theta}^H \tilde{\boldsymbol{\omega}}_k + x_c^* \tilde{h}_k \right) - |x_c|^2 \left(\sum_{i=1}^N \rho_{k,i} P_i^{d(j)} Q_i^w + \sigma^2 \right). \quad (28)$$

With $\boldsymbol{\theta}$ being fixed, $f_d(x_d, \boldsymbol{\theta}^{(j)})$ and $f_c(x_c, \boldsymbol{\theta}^{(j)})$ are concave differentiable functions over x_d and x_c , respectively. The optimal solution of x_d and x_c can be obtained by setting $\partial f_d(x_d, \boldsymbol{\theta}^{(j)}) / \partial x_d = 0$ and $\partial f_c(x_c, \boldsymbol{\theta}^{(j)}) / \partial x_c = 0$, respectively. The optimal values of x_d and x_c are obtained, respectively, as follows

$$x_{\text{opt},d}^{(j)} = \frac{\sqrt{P_n^{d(j)}} (\boldsymbol{\theta}^H \boldsymbol{\omega}_{n,n} + h_{n,n})}{\sum_{k=1}^K \rho_{k,n} P_k^{c(j)} \tilde{Q}_{n,k}^w + \sigma^2}. \quad (29)$$

$$x_{\text{opt},c}^{(j)} = \frac{\sqrt{P_k^{c(j)}}(\boldsymbol{\theta}^{H(j)}\tilde{\boldsymbol{\omega}}_k + \tilde{h}_k)}{\sum_{i=1}^N \rho_{k,i} P_i^{d(j)} Q_{b,i}^w + \sigma^2}. \quad (30)$$

Similarly, replacing $x_d^{(j)}$ and $x_c^{(j)}$ with $x_{\text{opt},d}^{(j)}$ and $x_{\text{opt},c}^{(j)}$, respectively, the following relationships are established

$$f_d(\boldsymbol{\theta}) = -\boldsymbol{\theta}^H \mathbf{B}_2 \boldsymbol{\theta} + 2\text{Re}(\boldsymbol{\theta}^H \mathbf{e}_2) + C_2 \geq \gamma_{\min}^d, \quad (31)$$

$$f_c(\boldsymbol{\theta}) = -\boldsymbol{\theta}^H \mathbf{B}_3 \boldsymbol{\theta} + 2\text{Re}(\boldsymbol{\theta}^H \mathbf{e}_3) + C_3 \geq \gamma_{\min}^c, \quad (32)$$

where the positive-definite matrixes \mathbf{B}_2 and \mathbf{B}_3 are given by

$$\mathbf{B}_2 = |x_{\text{opt},d}^{(j)}|^2 \mathbf{B}_{2n}, \quad (33)$$

$$\mathbf{B}_3 = |x_{\text{opt},c}^{(j)}|^2 \mathbf{B}_{2b}, \quad (34)$$

the vectors \mathbf{e}_2 and \mathbf{e}_3 are given by

$$\mathbf{e}_2 = \sqrt{P_n^{d(j)}}(x_{\text{opt},d}^{(j)})^* \boldsymbol{\omega}_{n,n} - |x_{\text{opt},d}^{(j)}|^2 \mathbf{e}_{2n}, \quad (35)$$

$$\mathbf{e}_3 = \sqrt{P_k^{c(j)}}(x_{\text{opt},c}^{(j)})^* \tilde{\boldsymbol{\omega}}_k - |x_{\text{opt},c}^{(j)}|^2 \mathbf{e}_{2b}, \quad (36)$$

and the constants C_2 and C_3 are given by

$$C_2 = 2\sqrt{P_n^{d(j)}} \text{Re} \left\{ (x_{\text{opt},d}^{(j)})^* h_{n,n} \right\} - |x_{\text{opt},d}^{(j)}|^2 \left(\sum_{k=1}^K \rho_{k,n} P_k^{c(j)} |v_{n,k}|^2 + \sigma^2 \right), \quad (37)$$

$$C_3 = 2\sqrt{P_k^{c(j)}} \text{Re} \left\{ (x_{\text{opt},c}^{(j)})^* \tilde{h}_k \right\} - |x_{\text{opt},c}^{(j)}|^2 \left(\sum_{i=1}^N \rho_{k,i} P_i^{d(j)} |u_i|^2 + \sigma^2 \right). \quad (38)$$

Therefore, (P1.2.T) is transformed as the following problem

$$\text{(P1.2.Q)} : \max_{\boldsymbol{\theta}} -\boldsymbol{\theta}^H \mathbf{B}_1 \boldsymbol{\theta} + 2\text{Re}(\boldsymbol{\theta}^H \mathbf{e}_1) + C_1 \quad (39a)$$

$$\text{s.t.} \quad (31), (32), (7h). \quad (39b)$$

The resulting (P1.2.Q) is a quadratic constrained quadratic programming (QCQP) problem, which can be effectively solved by standard toolbox, e.g., CVX [38].

D. Optimize Reflecting Coefficient matrix Φ with $\mathcal{F} = \mathcal{F}_2$

In this subsection, we solve (P1) with $\mathcal{F} = \mathcal{F}_2$, which makes (7h) a non-convex constraint. We utilize the projection method to solve this non-convex problem. For the convenience of illustration, the optimal solutions to (P1) with $\mathcal{F} = \mathcal{F}_1$ and with $\mathcal{F} = \mathcal{F}_2$ are denoted by $(\mathbf{p}_{\text{opt},1}, \Phi_{\text{opt},1})$ and $(\mathbf{p}_{\text{opt},2}, \Phi_{\text{opt},2})$ respectively.

Notice that $\mathbf{p}_{\text{opt},2}$ take the values of $\mathbf{p}_{\text{opt},1}$, i.e., $\mathbf{p}_{\text{opt},2} = \mathbf{p}_{\text{opt},1}$. To obtain a suboptimal $\Phi_{\text{opt},2}$, we project the solution to (P1) with $\mathcal{F} = \mathcal{F}_1$ into $\mathcal{F} = \mathcal{F}_2$. Specifically, we take the maximum value of the reflecting amplitude (i.e., $\alpha_m = 1$), and the reflecting phases of $\Phi_{\text{opt},2}$ take the same value of $\Phi_{\text{opt},1}$. Therefore, the solution to (P1) with $\mathcal{F} = \mathcal{F}_2$ can be written as

$$\Phi_{\text{opt},2} = e^{j \arg(\Phi_{\text{opt},1})}. \quad (40)$$

E. Optimize Reflecting Coefficient matrix Φ with $\mathcal{F} = \mathcal{F}_3$

In this subsection, we solve (P1) with $\mathcal{F} = \mathcal{F}_3$, which makes (P1) a non-convex combinational optimization problem. Such a problem is indeed NP-hard, and its complexity of exhaustive-search method increases exponentially as the number of reflecting elements increases. Similarly, we exploit the projection method to solve this non-convexity. Denote the optimal solutions to (P1) with $\mathcal{F} = \mathcal{F}_3$ by $(\mathbf{p}_{\text{opt},3}, \Phi_{\text{opt},3})$.

We project the solution to (P1) with $\mathcal{F} = \mathcal{F}_1$ into $\mathcal{F} = \mathcal{F}_3$. Specifically, we take the maximum value of the reflecting amplitude (i.e., $\alpha_m = 1$), and the reflecting phases of $\Phi_{\text{opt},3}$ take the nearest value of $\Phi_{\text{opt},1}$. Therefore, the solution to (P1) with $\mathcal{F} = \mathcal{F}_3$ can be written as

$$\theta_m = \arg \min_{\theta_m \in \{0, \frac{2\pi}{2^B}, \dots, \frac{2\pi(2^B-1)}{2^B}\}} |\theta_m - \arg(\Phi_m^{\text{opt},1})|, \quad (41)$$

where $\Phi_m^{\text{opt},1}$ denotes the m -th element on the diagonal line of $\Phi_{\text{opt},1}$. Similarly, $\mathbf{p}_{\text{opt},3}$ takes the value of $\mathbf{p}_{\text{opt},1}$, i.e., $\mathbf{p}_{\text{opt},3} = \mathbf{p}_{\text{opt},1}$.

F. Overall Algorithm

The overall algorithm is summarized in Algorithm 1. There are three blocks of variables to be optimized, i.e., ρ , \mathbf{p} and Φ . We first use a low-complexity user-pairing scheme based on the RCS to determine the resource reuse indicator vector ρ . Under the obtained user-pairing design, we use the AO algorithm to optimize \mathbf{p} and Φ alternatively in the out-layer iteration. Specifically, for given Φ ,

Algorithm 1 Proposed algorithm for solving (P1)

Step 1: Initialize $\mathbf{p}^{(0)}$, $\Phi^{(0)}$, a small threshold constant $\epsilon = 10^{-2}$. Let $j = 0$.

Step 2: Exploit RCS-based pairing scheme to determine the resource reuse indicator vector ρ^* .

repeat

Step 3: Solve problem (P1.1.A) for given $\Phi^{(j)}$, and obtain the optimal solution as $\mathbf{p}^{(j+1)}$.

Step 4: Solve problem (P1.2.Q) for given $\mathbf{p}^{(j+1)}$, and obtain the optimal solution as $\Phi^{(j+1)}$.

Step 5: Update iteration index $j = j + 1$.

until The increase of objective value is smaller than ϵ .

Step 6: Return the suboptimal solution ρ^* , $\mathbf{p}^* = \mathbf{p}^{(j-1)}$ and $\Phi^* = \Phi^{(j-1)}$.

we utilize the SCA technique to tackle the non-convexity of the objective function; for given \mathbf{p} , we exploit the Lagrangian dual transform technique to deal with the sum of logarithm function, then utilize the quadratic transform technique to solve the resulting multiple-ratio fractional programming problem.

G. Convergence and Complexity Analyses

1) *Convergence Analysis:* The convergence of Algorithm 1 is given in the following theorem.

Theorem 1. *Algorithm 1 is guaranteed to converge.*

Proof. First, in Step 3, since the suboptimal solution $\mathbf{p}^{(j+1)}$ is obtained for given $\Phi^{(j)}$, we have the following inequality on the sum rate

$$\begin{aligned}
 R(\mathbf{p}^{(j)}, \Phi^{(j)}) &\stackrel{(a)}{=} R^{\text{lb}}(\mathbf{p}^{(j)}, \Phi^{(j)}) \\
 &\stackrel{(b)}{\leq} R^{\text{lb}}(\mathbf{p}^{(j+1)}, \Phi^{(j)}) \\
 &\stackrel{(c)}{=} R(\mathbf{p}^{(j+1)}, \Phi^{(j)}),
 \end{aligned} \tag{42}$$

where (a) and (c) hold since the Taylor expansion in (11) is tight at given local point $\mathbf{p}^{(j)}$ and $\mathbf{p}^{(j+1)}$, respectively, and (b) comes from the fact that $\mathbf{p}^{(j+1)}$ is the optimal solution to problem (P1.1.A).

Second, in Step 4, since $\Phi^{(j+1)}$ is the optimal solution to problem (P1.2.Q), we can obtain the following inequality

$$R(\mathbf{p}^{(j+1)}, \Phi^{(j)}) \leq R(\mathbf{p}^{(j+1)}, \Phi^{(j+1)}). \tag{43}$$

From (42) and (43), it is straightforward that

$$R(\mathbf{p}^{(j)}, \Phi^{(j)}) \leq R(\mathbf{p}^{(j+1)}, \Phi^{(j+1)}), \quad (44)$$

which implies that the objective value of problem (P1) is non-decreasing after each iteration in Algorithm 1. In addition, the objective value of problem (P1) is upper-bounded by some finite positive number since the objective function is continuous over the compact feasible set. Hence, the proposed Algorithm 1 is guaranteed to converge. This completes the convergence proof. \square

2) *Complexity Analysis:* In Algorithm 1, the subproblems (P1.1.A) and (P1.2.Q) are alternatively solved in each outer-layer AO iteration, and the overall complexity of Algorithm 1 is mainly introduced by the update of the variables \mathbf{p} , Φ , \mathbf{y} , x_d and x_c . Notice that the optimal \mathbf{y} , x_d and x_c are all obtained in closed forms, thus the computational complexity is negligible. Specifically, (P1.1.A) can be solved in $\mathcal{O}((N + K)^3)$ operations [40], while (P1.2.Q) is a convex QCQP which can be solved using interior point methods with complexity $\mathcal{O}(M^{3.5})$ [41]. Hence, the complexity of Algorithm 1 is $\mathcal{O}(I_{\text{ite}}[(N + K)^3 + M^{3.5}])$, where I_{ite} denotes the number of outer-layer AO iterations.

V. ENERGY EFFICIENCY MAXIMIZATION

In this section, we maximize the EE of the overall network, by jointly optimizing the resource reuse indicator vector $\boldsymbol{\rho}$, the transmit power vector \mathbf{p} and the reflecting coefficients matrix Φ .

A. Problem Formulation for EE Maximization

Before formulating the EE-maximization problem, we model the power consumption of the RIS. Due to the passive reflecting characteristic, the RIS's power consumption mainly comes from the control circuits [33]. For typical control circuits, a field programmable gate array (FPGA) outputs digital control voltages with given sampling frequency, which are converted into analog control voltages by multiple digital-to-analog converters (DACs). The analog control voltage from each DAC adjusts the capacitance of each varactor diode in a continuous way, and thus controls the phase shift and amplitude of each element's reflected signals [33]. Hence, the power consumption of RIS is modeled as follows

$$P_{\text{RIS}}(B) = P_{\text{FPGA}} + MP_{\text{DAC}}(B) + MP_v(B), \quad (45)$$

where P_{FPGA} , $P_{\text{DAC}}(B)$ and $P_v(B)$ denote the power of the FPGA, a B -bit DAC, and a varactor diode with 2^B different bias voltages, respectively. From [42], the DAC's power $P_{\text{DAC}}(B) = 1.5 \times 10^{-5} \cdot 2^B + 9 \times 10^{-12} \cdot B \cdot f_s$, where f_s is the sampling frequency. The varactor-diode power¹ $P_v(B) = \mathbb{E}_{v_b \in \mathcal{V}}[v_b i_r]$, where $\mathcal{V} = \{V_1, V_2, \dots, V_{2^B}\}$ is the set of designed bias voltages.

Hence, the EE-maximization optimization problem is formulated as

$$(P2) : \max_{\rho, \mathbf{p}, \Phi} \frac{R(\rho, \mathbf{p}, \Phi)}{\sum_{k=1}^K P_k^c + \sum_{n \in \mathcal{D}} P_n^d + (K + 2N + 1)P_0 + P_{\text{RIS}}(B)} \quad (46a)$$

$$\text{s.t. } (7b), (7c), (7d), (7e), (7f), (7g), (7h), \quad (46b)$$

where $\sum_{k=1}^K P_k^c$ and $\sum_{n \in \mathcal{D}} P_n^d$ are the total transmit power of CUs and D2D transmitters, respectively, and P_0 is the circuit-power consumption at each transmitter or receiver of the overall network.

The constraints of (P2) which are the same as in (P1) are non-convex, and the objective function of (P2) is a fractional non-convex function with respect to the power allocation variables \mathbf{p} . Hence, there is no standard method to solve (P2).

B. Solution to (P2)

To solve (P2), we first determine ρ through the RCS-based user-pairing scheme. Then, the variables \mathbf{p} and Φ are decoupled through AO technique.

1) *Solution to Subproblems:* In each iteration j , for given reflecting coefficient matrix $\Phi^{(j)}$, the transmit power vector \mathbf{p} can be optimized by solving the following subproblem

$$(P2.1) : \max_{\mathbf{p}} \frac{R(\mathbf{p})}{\sum_{k=1}^K P_k^c + \sum_{n \in \mathcal{D}} P_n^d + (K + 2N + 1)P_0 + P_{\text{RIS}}(B)} \quad (47a)$$

$$\text{s.t. } (7b), (7c), (7f), (7g). \quad (47b)$$

We utilize the SCA technique as mentioned before to tackle the non-convexity of the numerator in (47a), then transform it through the fractional programming into a parametric subtractive form with an introduced parameter λ , and exploit Dinkelbach's method [43] to obtain a solution of λ and \mathbf{p} . The solving sub-algorithm based on Dinkelbach's method is summarized in Algorithm 2.

¹Notice that $P_v(B)$ is negligible in practice, since the current of a varactor diode in the reversely-biased (until reverse breakdown) working status is almost constant and very small (typically, tens of nanoAmperes (nA)).

Algorithm 2 Proposed algorithm for solving (P2)

Step 1: Initialize $\mathbf{p}^{(0)}$, $\Phi^{(0)}$, $\lambda^{(0)} = 0$, permissible error $\delta = 10^{-3}$, a small threshold constant $\epsilon = 10^{-2}$. Let $i = 0$, $j = 0$.

Step 2: Exploit RCS-based pairing scheme to determine the resource reuse indicator vector ρ^* .
repeat

Step 3: Solve problem (P2.1) for given $\Phi^{(j)}$, and obtain the optimal solution as $\mathbf{p}^{(j+1)}$.

repeat

3.1: Solve the following optimization problem to obtain the optimal transmit power
 $\mathbf{p}^{*(i)}: \max_{\mathbf{p}} f(\lambda^{(i)}) = R^{\text{lb}(i)} - \lambda^{(i)} \left(\sum_{k=1}^K P_k^{c(i)} + \sum_{n \in \mathcal{D}} P_n^{d(i)} + (K + 2N + 1)P_0 + P_{\text{RIS}}(B) \right)$

3.2: Update the introduced parameter with $\lambda^{(i)} = \frac{R^{\text{lb}(i)}(\mathbf{p}^{*(i)})}{\sum_{k=1}^K P_k^{c*(i)} + \sum_{n \in \mathcal{D}} P_n^{d*(i)} + (K + 2N + 1)P_0 + P_{\text{RIS}}(B)}$

3.3: Update iteration index $i = i + 1$.

until $f(\lambda) < \delta$

return $\mathbf{p}^{(j+1)} = \mathbf{p}^{*(i-1)}$.

Step 4: Solve problem (P2.2) for given $\mathbf{p}^{(j+1)}$, and obtain the optimal solution as $\Phi^{(j+1)}$.

Step 5: Update iteration index $j = j + 1$.

until The increase of objective value is smaller than ϵ .

Step 6: Return the suboptimal solution ρ^* , $\mathbf{p}^* = \mathbf{p}^{(j-1)}$ and $\Phi^* = \Phi^{(j-1)}$.

For given transmit power vector $\mathbf{p}^{(j)}$, the reflecting coefficient matrix Φ can be optimized by solving the following subproblem

$$(P2.2): \max_{\Phi} \frac{R(\Phi)}{\sum_{k=1}^K P_k^{c(j)} + \sum_{n \in \mathcal{D}} P_n^{d(j)} + (K + 2N + 1)P_0 + P_{\text{RIS}}(B)} \quad (48a)$$

$$\text{s.t. } (7b), (7c), (7h). \quad (48b)$$

Since the denominator in the objective function is a constant, this subproblem (P2.2) can be solved in the same way as in IV-C to obtain a solution to Φ .

2) *Overall Algorithm and Analyses:* The overall algorithm for solving (P2) is summarized in Algorithm 2. Specifically, the Dinkelbach-based Algorithm 2 is used to solve subproblem (P2.1) in Step 3, and the subproblem (P2.2) is solved in Step 4. The subproblem (P2.1) and (P2.2) are alternatively solved in each outer-layer iteration.

The convergence of Algorithm 2 can be proved by similar steps as in the proof of Theorem 1, thus omitted herein, since the Dinkelbach's method converges superlinearly for nonlinear fractional programming problems [43].

The proposed Dinkelbach's method solves a convex optimization problem in each iteration, thus

the complexity of each iteration is $\mathcal{O}(\log_2(\frac{1}{\epsilon}))$. The complexity for solving (P2.1) with permissible error δ is $\mathcal{O}(\frac{1}{\delta^2} \log_2(\frac{1}{\epsilon}) \log_2(N + K))$ [43]. (P2.2) can be transformed as a convex QCQP which can be solved using interior point methods with complexity $\mathcal{O}(M^{3.5})$ [41]. Hence, the complexity of Algorithm 2 is $\mathcal{O}(I_{\text{ite}} [\frac{1}{\delta^2} \log_2(\frac{1}{\epsilon}) \log_2(N + K) + M^{3.5}])$, where I_{ite} denotes the number of outer-layer AO iterations.

VI. NUMERICAL RESULTS

This section provides numerical results for the RIS-empowered D2D underlying cellular network, which show significant performance enhancement of the proposed design as compared to the conventional underlying D2D network without RIS and other benchmarks.

A. Simulation Setups

Each channel response consists of a large-scale fading component and a small-scale fading component. Without loss of generality, the large-scale fading is distance-dependent and can be modeled as $Cd^{-\alpha}$, where d is the distance between transmitter and receiver with unit of meter (m), $C = 10^{-3}$ is the path loss at the reference distance of 1 m, and α is the path loss exponent of the channel. The path loss exponents from TXs/CUs to RXs/BS are 4, from IRS to BS is 2, the others of RIS-related channels are 2.2 [14] [33]. The small-scale fading components of $h_{l,i}$, u_i , \tilde{h}_k and $v_{l,k}$ are considered as independently Rayleigh fading distributed, while the small-scale fading components of \mathbf{f}_i , $\tilde{\mathbf{f}}_k$, \mathbf{g}_l and $\tilde{\mathbf{g}}$ follow independent Rician fading distribution, i.e.,

$$\mathbf{f}_i = \sqrt{\frac{K_1}{K_1 + 1}} \mathbf{f}_{L,i} + \sqrt{\frac{1}{K_1 + 1}} \mathbf{f}_{N,i}, \quad (49)$$

where K_1 is the Rician factor of \mathbf{f}_i , $\mathbf{f}_{L,i}$ is the line of sight (LoS) component, and $\mathbf{f}_{N,i}$ is the non-LoS (NLOS) component where each element follows CSCG distribution $\mathcal{CN}(0, 1)$. Similarly, $\tilde{\mathbf{f}}_k$, \mathbf{g}_l and $\tilde{\mathbf{g}}$ are generated in the same way as \mathbf{f}_i with Rician factors K_2 , K_3 and K_4 , respectively. Rician factors are set as the same value, i.e., $K_1 = K_2 = K_3 = K_4 = 10$.

We assume that the CUs are uniformly distributed in the cellular cell with radius $R = 250$ m. We adopt the clustered distribution model in [14] for D2D users, i.e., the clusters are randomly located in the cell, and each D2D link is uniformly distributed in one cluster with radius $r = 60$ m. We set $K = 4$ and $N = 2$. The RIS is located between two D2D clusters. Using the above method, the locations of CUs and D2D users are generated by one realization, as illustrated in Fig. 2, and then fixed in all the simulations. The coordinates of CU 1, CU 2, CU 3 and CU 4 are (38, 54), (87, 92),

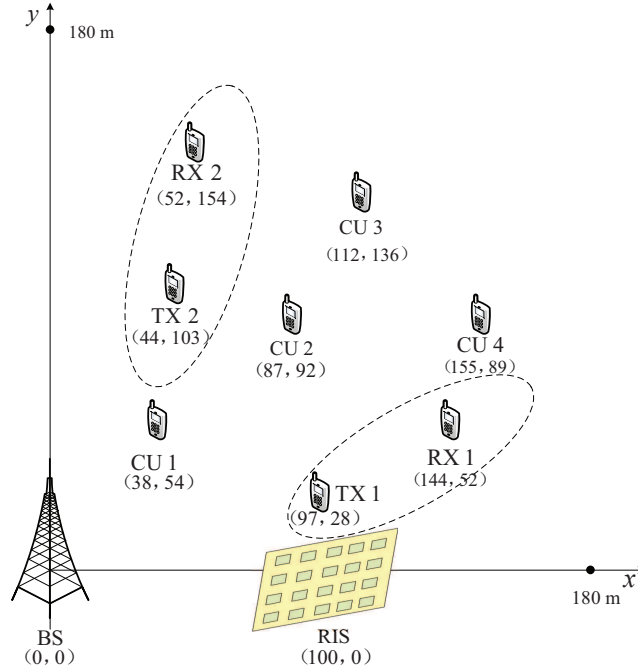


Fig. 2: Topology of RIS-empowered underlying D2D communication network.

TABLE I: Parameter settings.

Cellular cell radius	250 m
D2D cluster radius	60 m
Number of reflecting elements	$M = 200$
Number of CUs	$K = 4$
Number of D2D pairs	$N = 2$
D2D TXs' maximum transmit power	$P_{\max}^d = 24$ dBm
CUs' maximum transmit power	$P_{\max}^c = 24$ dBm
D2D RXs' minimum SINR requirement	$R_{\min}^d = 0.3$ bps/Hz
CUs' minimum SINR requirement	$R_{\min}^c = 0.3$ bps/Hz
Noise power	$\sigma^2 = -114$ dBm
Channel realizations	1000

(112, 136) and (155, 89), respectively; the coordinates of TX 1 and RX 1 are (97, 28), (144, 52), respectively; the coordinates of TX 2 and RX 2 are (44, 103), (52, 154), respectively; the coordinate of RIS is (100, 0). We set $\sigma^2 = -114$ dBm [14]. Moreover, each antenna at the users is assumed to have an isotropic radiation pattern with 0 dB antenna gain, while each reflecting element of IRS is assumed to have 3 dB gain for fair comparison, since each IRS reflects signals only in its front half-space. The simulation results are based on 1000 channel realizations. Parameter settings are summarized in Table I.

B. Benchmark Schemes

For comparison, we consider the following three benchmark schemes.

1) *Underlying D2D Without RIS*: The traditional RIS-empowered D2D underlying cellular network without RIS is considered. The SE and EE are maximized by jointly optimizing the resource reuse indicator ρ and transmit power vector \mathbf{p} . The solving algorithm in [14] is used and omitted.

2) *Proposed Design with Random Reflecting Coefficients*: The proposed design without optimizing the reflecting coefficients matrix Φ is considered. We maximize the SE and EE by jointly optimizing ρ and \mathbf{p} . All reflecting elements are set with random phase and maximal amplitude. This benchmark is used to show the benefit of passive beamforming optimization.

3) *RIS-Empowered D2D With Ideal User Pairing*: We exhaustively search over A_K^N possible user pairings, and jointly optimize \mathbf{p} as well as Φ under each pairing. This benchmark gives achievable upper-bound performance of the RIS-empowered underlying D2D network.

C. Simulation Analyses for SE Maximization

In this subsection, we evaluate the SE performance. We set $M = 200$, $P_{\max}^d = P_{\max}^c = 24$ dBm [14], $R_{\min}^d = \log_2(1 + \gamma_{\min}^d) = 0.3$ bps/Hz, $R_{\min}^c = \log_2(1 + \gamma_{\min}^c) = 0.3$ bps/Hz, $P_{\max}^d = P_{\max}^c = P_{\max}$, if being not specified locally for some specific figure.

Fig. 3 plots the SE versus the maximum transmit power P_{\max} for the proposed design and different benchmarks. As shown in Fig. 3, the proposed design achieves significant SE enhancement compared to the first benchmark. For instance, the SE of the proposed design is 77.42% and 73.8% higher than that of the first benchmark, for $P_{\max} = 20, 30$ dBm, respectively. Also, the proposed design outperforms the second benchmark without optimizing Φ , which shows the benefit of passive beamforming optimization. Compared to the third benchmark, the proposed design suffers from slight SE performance degradation, but obviously outperforms this benchmark in terms of computational complexity. The proposed design solves the joint-resource-allocation optimization problem only once, while this benchmark needs to solve such problem for A_K^N times under all possible pairings, resulting into unaffordable complexity especially for large numbers of D2D or cellular links.

Fig. 4 plots the SE versus the maximum transmit power P_{\max} for the proposed design with different reflecting coefficients settings. First, it is observed that the finite-resolution phase shifters of the reflecting elements usually degrades the SE performance. The SE increases with the increase of the phase-shift quantization bits B , since the increase of B makes the setting of reflecting coefficients

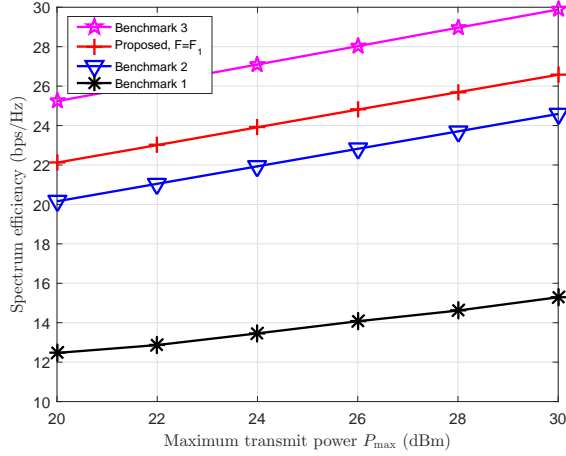


Fig. 3: SE versus P_{\max} for proposed design and

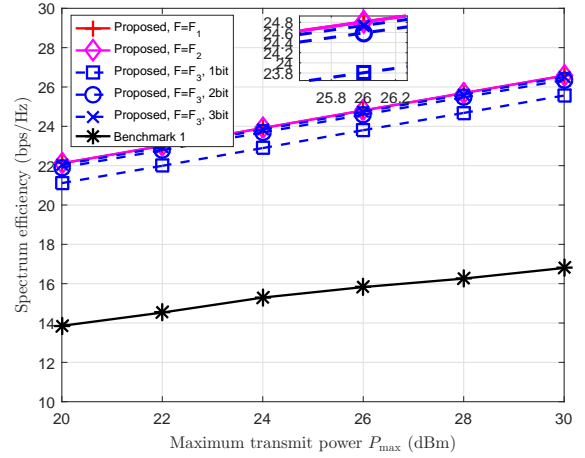


Fig. 4: SE versus P_{\max} for proposed design with different reflecting coefficients settings.

more accurate. In particular, the 2-bit phase shifter can obtain sufficiently high performance gain with a slight performance degradation compared to the ideal case of continuous phase shifters. Furthermore, the SE of the proposed design with $\mathcal{F} = \mathcal{F}_2$ is almost the same as the proposed design with $\mathcal{F} = \mathcal{F}_1$. The reason is as follows. As long as the reflecting amplitudes take the maximal value, channel strength enhancement and inter-link interference suppression can be achieved to the greatest extent by adjusting the reflecting phase shifts.

Fig. 5 plots the SE versus the number of reflecting elements M of the RIS. First, the SE of proposed designs increases as M increases, since more reflecting elements can further enhance equivalent channel strength and suppress the inter-link interference; while the SE of first benchmark almost remains unchanged. Then, we observe that the gap between the proposed design and the second benchmark enlarges with the increase of M , since more reflecting elements are well designed to achieve better performance for the proposed design, while the reflecting elements of the second benchmark stay initial random values. Moreover, compared to the third benchmark with extremely high complexity, the proposed design achieves 79.67% and 88.94% SE performance of the third benchmark (upper bound) when M is 50 and 400, respectively.

Fig. 6 plots the SE versus the CUs' minimum rate requirement R_{\min}^c . The SE decreases as R_{\min}^c increases, which reveals the rate tradeoff between D2D links and cellular links. The proposed design achieves significant SE enhancement by introducing an RIS as compared to the first benchmark for $R_{\min}^c \leq 1.5$ bps/Hz. For $R_{\min}^c \geq 1.5$ bps/Hz, the first benchmark achieves higher SE as compared

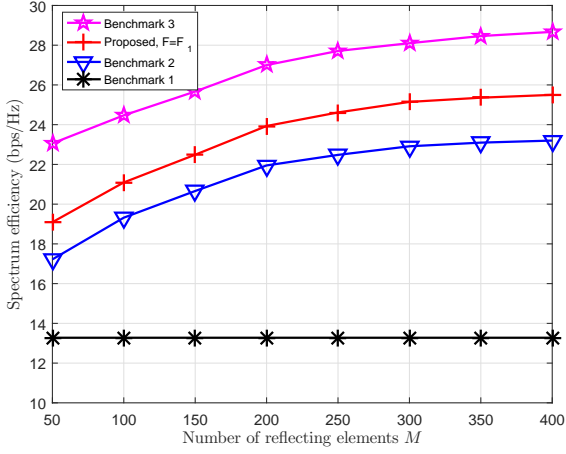


Fig. 5: SE versus RIS's number of reflecting elements M .

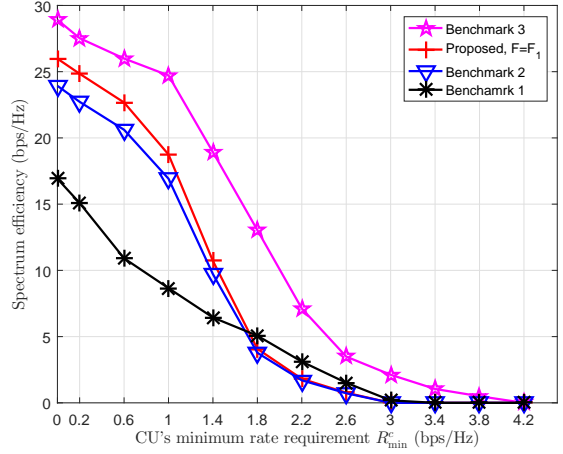


Fig. 6: SE versus CU's minimum rate requirement R_{\min}^c .

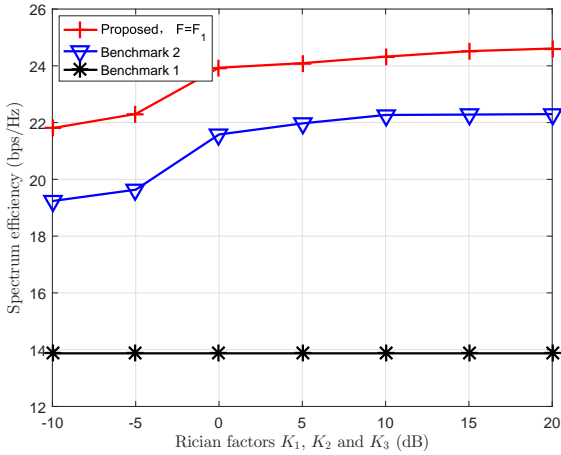


Fig. 7: SE versus Rician factors K_1 , K_2 and K_3 .

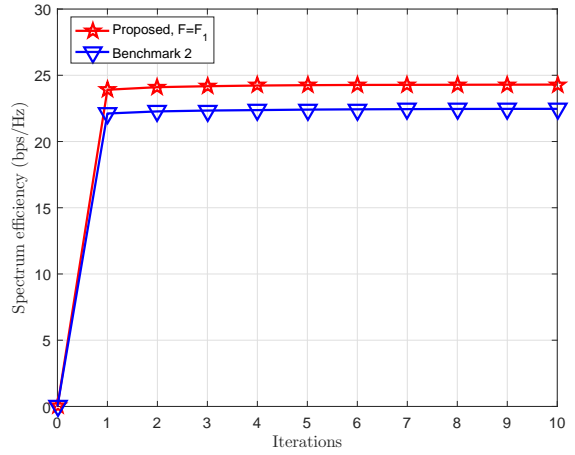


Fig. 8: Convergence of Algorithm 1 for (P1).

to the proposed design. The reason is that both the pairing scheme and the benefits introduced by the RIS affect the SE performance. When R_{\min}^c is relatively small, the proposed design with a suboptimal pairing scheme is able to obtain a feasible solution, the performance enhancement comes from the well-designed RIS; in contrast, when R_{\min}^c is too large, the formulated problem is not likely to be solved under a suboptimal pairing scheme, which results into worse performance of the proposed design as compared to the first benchmark with ideal pairing scheme.

Fig. 7 plots the the SE versus the Rician factors K_1 , K_2 and K_3 . It is observed that the SE of the proposed design increases as Rician factors increase, since the increase of K_1 , K_2 and K_3 indicates that the LoS components between users and RIS are enhanced, thus reduces the depth of

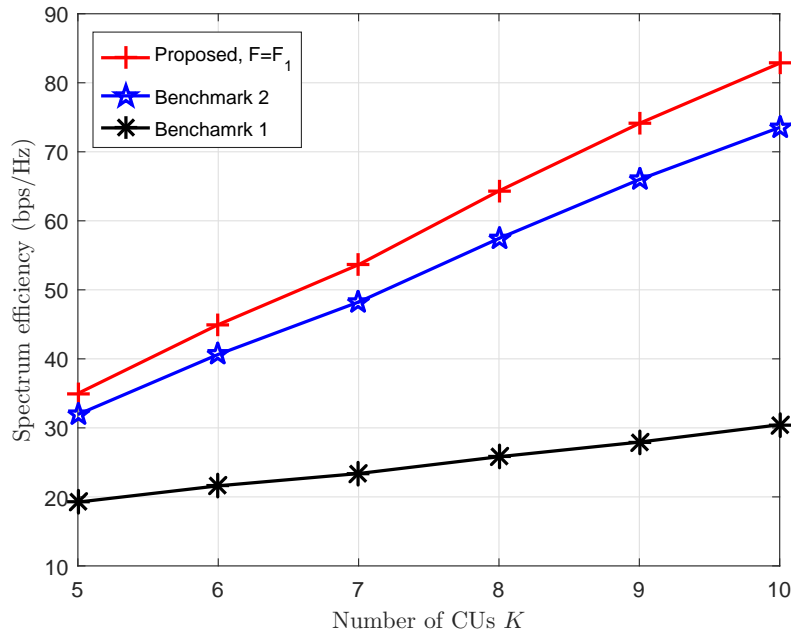


Fig. 9: SE versus number of CUs K .

signal fading. The SE of first benchmark almost remains unchanged. Furthermore, the slope of the curve decreases with the increase of Rician factors. When Rician factors are small, NLoS path is dominant and the increase of Rician factors means the increase of LoS-path strength; when Rician factors are relatively large, LoS path is absolutely dominant thus the increase of Rician factors has less effect on the channel strength.

Fig. 8 plots the average convergence performance of the proposed Algorithm 1. We observe that the proposed scheme takes about five iterations to converge. The converged average SE is 24.34 bps/Hz and 22.482 bps/Hz for the proposed design and the second benchmark, respectively. Thus, the convergence speed of Algorithm 1 is fast.

Fig. 9 plots the SE versus the number of CUs. We set the coordinates of added CUs as (99, 44), (122, 174), (138, 162), (74, 121), (56, 112) and (149, 78), respectively. The proposed design significantly outperforms the first benchmark when the number of CUs is relatively large. For example, the SE of the proposed design is 81.82% and 172% higher than that of the first benchmark when the number of CUs is 5 and 10 respectively. The reason is explained as follows. With the number of CUs increases, the SE performance for the first benchmark only benefits from the potential better pairing and the rate of added CUs, while the SE performance for the proposed design also

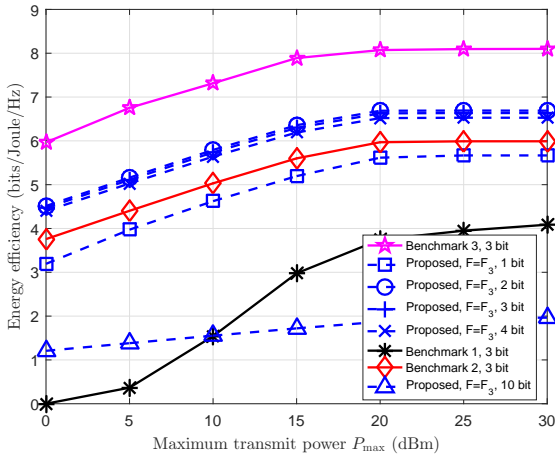


Fig. 10: EE versus D2D TXs' maximum transmit power P_{\max} .

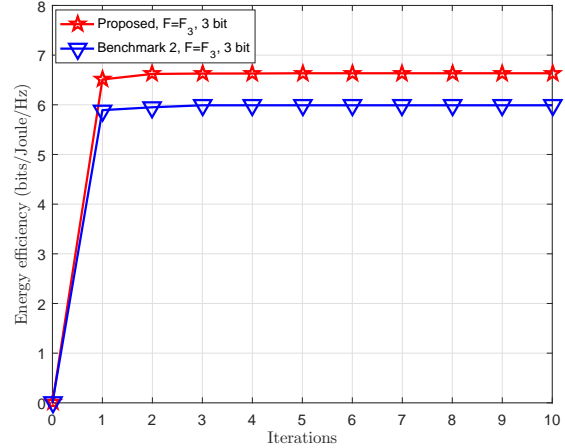


Fig. 11: Convergence of Dinkelbach-based Algorithm 2 for (P2).

benefits from the enhancement of the RIS.

D. Simulation Analyses for EE Maximization

In this subsection, we evaluate the EE performance. As in [44], we take the diode SMV1231-079 with inverse current i_r less than 20 nA, and estimate the power $P_v(B)$ for different B 's. We take the typical Xilinx Spartan-7 FPGA for consideration, and use its typical power $P_{\text{FPGA}} = 1.188\text{W}$. The average power consumption of each reflecting element for different quantization bit B with reflecting-element number M is given in Table II. In the simulations, we set $M = 500$, $R_{\min}^d = R_{\min}^c = 0.55$ bps/Hz, $P_r = 24$ dBm, and $f_s = 10$ KHz. The bias voltages of varactor diode are chosen in the range of [0.12, 8.83]. Other settings remain unchanged as in subsection VI-C.

TABLE II: Power consumption (mW) of each reflecting element.

$M \backslash B$	1	2	3	4	5	6	7	8	9	10
200	5.970	6.000	6.060	6.180	6.420	6.900	7.860	9.780	13.620	21.300
500	2.406	2.436	2.496	2.616	2.856	3.336	4.296	6.216	10.056	17.736
1000	1.218	1.248	1.308	1.428	1.668	2.148	3.108	5.028	8.868	16.548

Fig. 10 plots the EE versus the maximum transmit power P_{\max} . It is observed that EE increases as P_{\max} increases first, then almost remains unchanged for large P_{\max} , since the increment of SE is not as fast as the increment of consumed power. The proposed design significantly outperforms the first benchmark with 3-bit phase shifts. As the number of phase-shift quantization bits B increases,

the EE increases first and then decreases slowly, with the optimal EE at $B = 2$. The reason is that despite the increase of B makes the setting of reflecting coefficients more accurate, but it results into higher power consumption simultaneously. When $B > 1$, the SE improvement from RIS is not enough to compensate for the increase of power consumption as B increases. In addition, the proposed design outperforms the second benchmark, due to the benefit of passive beamforming. Moreover, the proposed design suffers from slight EE performance degradation, but outperforms this benchmark in terms of computational complexity.

Fig. 11 plots the average convergence performance of Dinkelbach-based Algorithm 2 for solving EE-maximization problem (P2). We observe that the proposed design takes about five iterations to converge. The converged average EE is 6.35 bps/Joule/Hz and 5.99 bps/Joule/Hz for the proposed design and the second benchmark, respectively. Thus, the convergence of Algorithm 2 is fast.

VII. CONCLUSION

This paper has studied an RIS-empowered underlying D2D communication network. The overall network's spectrum efficiency (SE) and energy efficiency (EE) are maximized, respectively, by jointly optimizing the resource reuse indicators, the transmit power and the passive beamforming. First, an efficient relative-channel-strength based user-pairing scheme with low complexity is proposed to determine the resource reuse indicators. Then, the transmit power and the passive beamforming are jointly optimized for maximizing SE and EE, respectively, by utilizing the proposed alternating-optimization based iterative algorithms. Numerical results show that the proposed design achieves significant performance enhancement compared to traditional underlying D2D network without RIS, and suffers from slight performance degradation compared to RIS-empowered underlying D2D with ideal user-pairing. This work can be extended to practical and complex scenarios such as multi-antenna BS/users, multiple RISs, and imperfect/partial channel state information.

REFERENCES

- [1] F. Jameel, Z. Hamid, F. Jabeen, S. Zeadally, and M. A. Javed, "A survey of device-to-device communications: Research issues and challenges," *IEEE Commun. Sur. & Tut.*, vol. 20, no. 3, pp. 2133–2168, 2018.
- [2] A. Ghosh, A. Maeder, M. Baker, and D. Chandramouli, "5G evolution: A view on 5G cellular technology beyond 3GPP release 15," *IEEE Access*, vol. 7, pp. 127 639–127 651, 2019.
- [3] N. Naderializadeh and A. S. Avestimehr, "ITLinQ: A new approach for spectrum sharing in device-to-device communication systems," *IEEE J. Sel. Areas Commun.*, vol. 32, no. 6, pp. 1139–1151, 2014.
- [4] Y.-C. Liang, *Dynamic Spectrum Management: From Cognitive Radio to Blockchain and Artificial Intelligence*, ser. Signals and Communication Technology. Singapore: Springer, 2020.

- [5] H. Sun, M. Wildemeersch, M. Sheng, and T. Q. S. Quek, "D2D enhanced heterogeneous cellular networks with dynamic TDD," *IEEE Trans. Wireless Commun.*, vol. 14, no. 8, pp. 4204–4218, 2015.
- [6] J. Wang, Y. Huang, S. Jin, R. Schober, X. You, and C. Zhao, "Resource management for device-to-device communication: A physical layer security perspective," *IEEE J. Sel. Areas Commun.*, vol. 36, no. 4, pp. 946–960, 2018.
- [7] K. Yang, S. Martin, C. Xing, J. Wu, and R. Fan, "Energy-efficient power control for device-to-device communications," *IEEE J. Sel. Areas Commun.*, vol. 34, no. 12, pp. 3208–3220, 2016.
- [8] Y. Chen, B. Ai, Y. Niu, K. Guan, and Z. Han, "Resource allocation for device-to-device communications underlying heterogeneous cellular networks using coalitional games," *IEEE Trans. Wireless Commun.*, vol. 17, no. 6, pp. 4163–4176, 2018.
- [9] C. Liaskos, S. Nie, A. Tsioliaridou, A. Pitsillides, S. Ioannidis, and I. Akyildiz, "A new wireless communication paradigm through software-controlled metasurfaces," *IEEE Commun. Mag.*, vol. 56, no. 9, pp. 162–169, 2018.
- [10] M. Di Renzo, M. Debbah, and et. al., "Smart radio environments empowered by reconfigurable AI meta-surfaces: an idea whose time has come," *EURASIP J. Wireless Commun. Netw.*, vol. 2019, no. 1, pp. 1–20, 2019.
- [11] Y.-C. Liang, R. Long, Q. Zhang, J. Chen, H. V. Cheng, and H. Guo, "Large intelligent surface/antennas (LISA): Making reflective radios smart," *J. Commun. Inf. Netw.*, vol. 4, no. 2, pp. 40–50, 2019.
- [12] C. Huang, S. Hu, G. C. Alexandropoulos, A. Zappone, C. Yuen, R. Zhang, M. Di Renzo, and M. Debbah, "Holographic MIMO surfaces for 6G wireless networks: Opportunities, challenges, and trends," *IEEE Wireless Commun.*, Doi: 10.1109/MWC.001.1900534, 2020.
- [13] C.-H. Yu, K. Doppler, C. B. Ribeiro, and O. Tirkkonen, "Resource sharing optimization for device-to-device communication underlying cellular networks," *IEEE Trans. Wireless Commun.*, vol. 10, no. 8, pp. 2752–2763, 2011.
- [14] D. Feng, L. Lu, Y. Yuan-Wu, G. Y. Li, G. Feng, and S. Li, "Device-to-device communications underlying cellular networks," *IEEE Trans. Commun.*, vol. 61, no. 8, pp. 3541–3551, 2013.
- [15] Y. Kai, J. Wang, H. Zhu, and J. Wang, "Resource allocation and performance analysis of cellular-assisted OFDMA device-to-device communications," *IEEE Trans. Wireless Commun.*, vol. 18, no. 1, pp. 416–431, 2019.
- [16] J. Mirza, G. Zheng, K. Wong, and S. Saleem, "Joint beamforming and power optimization for D2D underlying cellular networks," *IEEE Trans. Veh. Technol.*, vol. 67, no. 9, pp. 8324–8335, 2018.
- [17] W. Cui, K. Shen, and W. Yu, "Spatial deep learning for wireless scheduling," *IEEE J. Sel. Areas Commun.*, vol. 37, no. 6, pp. 1248–1261, 2019.
- [18] F. Wang, C. Xu, L. Song, and Z. Han, "Energy-efficient resource allocation for device-to-device underlay communication," *IEEE Trans. Wireless Commun.*, vol. 14, no. 4, pp. 2082–2092, 2015.
- [19] D. Feng, G. Yu, C. Xiong, Y. Yuan-Wu, G. Y. Li, G. Feng, and S. Li, "Mode switching for energy-efficient device-to-device communications in cellular networks," *IEEE Tran. Wireless Commun.*, vol. 14, no. 12, pp. 6993–7003, 2015.
- [20] Y. J. Chun, S. L. Cotton, H. S. Dhillon, A. Ghayeb, and M. O. Hasna, "A stochastic geometric analysis of device-to-device communications operating over generalized fading channels," *IEEE Trans. Wireless Commun.*, vol. 16, no. 7, pp. 4151–4165, 2017.
- [21] Y. Wang, Y.-P. Hong, and W. Chen, "Dynamic transmission policy for multi-pair cooperative device-to-device communication with block-diagonalization precoding," *IEEE Trans. Wireless Commun.*, vol. 18, no. 6, pp. 3034–3048, 2019.
- [22] D. D. Penda, R. Wichman, T. Charalambous, G. Fodor, and M. Johansson, "A distributed mode selection scheme for full-duplex device-to-device communication," *IEEE Trans. Veh. Technol.*, vol. 68, no. 10, pp. 10 267–10 271, 2019.
- [23] A. Tang, X. Wang, and C. Zhang, "Cooperative full duplex device to device communication underlying cellular networks," *IEEE Trans. Wireless Commun.*, vol. 16, no. 12, pp. 7800–7815, 2017.

- [24] M. Mozaffari, W. Saad, M. Bennis, and M. Debbah, "Unmanned aerial vehicle with underlaid device-to-device communications: Performance and tradeoffs," *IEEE Trans. Wireless Commun.*, vol. 15, no. 6, pp. 3949–3963, 2016.
- [25] M. Di Renzo, A. Zappone, M. Debbah, M.-S. Alouini, C. Yuen, J. de Rosny, and S. Tretyakov, "Smart radio environments empowered by reconfigurable intelligent surfaces: How it works, state of research, and road ahead," *arXiv preprint arXiv:2004.09352*, 2020.
- [26] E. Björnson, O. Özdogan, and E. G. Larsson, "Intelligent reflecting surface versus decode-and-forward: How large surfaces are needed to beat relaying?" *IEEE Wireless Communications Letters*, vol. 9, no. 2, pp. 244–248, 2020.
- [27] G. Yang, Y.-C. Liang, R. Zhang, and Y. Pei, "Modulation in the air: Backscatter communication over ambient OFDM carrier," *IEEE Trans. Commun.*, vol. 66, no. 3, pp. 1219–1233, Mar. 2018.
- [28] G. Yang, Q. Zhang, and Y.-C. Liang, "Cooperative ambient backscatter communications for green Internet-of-Things," *IEEE Internet of Things J.*, vol. 5, no. 2, pp. 1116–1130, Apr. 2018.
- [29] H. Guo, Y.-C. Liang, J. Chen, and E. G. Larsson, "Weighted sum-rate maximization for reconfigurable intelligent surface aided wireless networks," *IEEE Tran. Wireless Commun.*, vol. 19, no. 5, pp. 3064–3076, 2020.
- [30] C. Huang, R. Mo, and C. Yuen, "Reconfigurable intelligent surface assisted multiuser miso systems exploiting deep reinforcement learning," *IEEE J. Sel. Areas Commun. (Early Access)*, 2020.
- [31] M. Jung, W. Saad, Y. Jang, G. Kong, and S. Choi, "Reliability analysis of large intelligent surfaces (LISs): Rate distribution and outage probability," *IEEE Wireless Commun. Lett.*, vol. 8, no. 6, pp. 1662–1666, 2019.
- [32] G. Yang, X. Xu, and Y.-C. Liang, "Intelligent reflecting surface assisted non-orthogonal multiple access," in *IEEE Wireless Commun. Netw. Conf. (WCNC), Seoul, Korea (South)*, 2020.
- [33] C. Huang, A. Zappone, G. C. Alexandropoulos, M. Debbah, and C. Yuen, "Reconfigurable intelligent surfaces for energy efficiency in wireless communication," *IEEE Trans. Wireless Commun.*, vol. 18, no. 8, pp. 4157–4170, 2019.
- [34] J. Chen, Y.-C. Liang, Y. Pei, and H. Guo, "Intelligent reflecting surface: A programmable wireless environment for physical layer security," *IEEE Access*, vol. 7, pp. 82 599–82 612, 2019.
- [35] G. Yang, Y. Liao, Y.-C. Liang, and O. Tirkkonen, "Reconfigurable intelligent surface empowered underlaying device-to-device communication," submitted to 2020 IEEE Global Communications Conference, available: <https://arxiv.org/abs/2006.02103>.
- [36] A. Ramezani-Kebrya, M. Dong, B. Liang, G. Boudreau, and S. H. Seyedmehdi, "Joint power optimization for device-to-device communication in cellular networks with interference control," *IEEE Trans. Wireless Commun.*, vol. 16, no. 8, pp. 5131–5146, 2017.
- [37] A. Beck, A. Ben-Tal, and L. Tretushvili, "A sequential parametric convex approximation method with applications to nonconvex truss topology design problems," *J. Global Opt.*, vol. 47, no. 1, pp. 29–51, 2010.
- [38] M. Grant, S. Boyd, and Y. Ye, "CVX: Matlab software for disciplined convex programming," 2008.
- [39] K. Shen and W. Yu, "Fractional programming for communication systems I: power control and beamforming," *IEEE Trans. Signal Processing*, vol. 66, no. 10, pp. 2616–2630, 2018.
- [40] D. Bharadia, G. Bansal, P. Kaligineedi, and V. K. Bhargava, "Relay and power allocation schemes for OFDM-based cognitive radio systems," *IEEE Trans. Wireless Commun.*, vol. 10, no. 9, pp. 2812–2817, 2011.
- [41] A. Hassanien, S. A. Vorobyov, and K. M. Wong, "Robust adaptive beamforming using sequential quadratic programming: An iterative solution to the mismatch problem," *IEEE Signal Processing Lett.*, vol. 15, pp. 733–736, 2008.
- [42] L. N. Ribeiro, S. Schwarz, M. Rupp, and A. L. F. de Almeida, "Energy efficiency of mmwave massive MIMO precoding with low-resolution DACs," *IEEE J. Sel. Topics in Sig. Proc.*, vol. 12, no. 2, pp. 298–312, 2018.
- [43] J.-P. Crouzeix and J. A. Ferland, "Algorithms for generalized fractional programming," *Math. Programm.*, vol. 52, no. 1-3, pp. 191–207, 1991.

- [44] S. Abeywickrama, R. Zhang, Q. Wu, and C. Yuen, "Intelligent reflecting surface: Practical phase shift model and beamforming optimization," *to appear in IEEE Trans. Commun.*, available at arxiv.org/abs/2002.10112, 2020.